

Monolithic stirrer reactor: The selective lactose oxidation in liquid phase over Au/Al₂O₃ nanostructured catalysts.

Authors:

S.A.Regenhardt¹, C.I.Meyer¹, O.Sanz², V.Sebastian³, S. Ivanova⁴, M.A. Centeno⁴, J.A. Odriozola⁴, M. Montes², A. J. Marchi¹, T.F.Garetto^{1,*}

¹GICIC (Catalysis Science and Engineering Research Group) – INCAPE (UNL-CONICET), Colectora Ruta Nac. N° 168 Km 0 (3000) Santa Fe, Argentina.

²Department of Applied Chemistry, Faculty of Chemistry, University of Basque Country (UPV/EHU), 20018 - San Sebastián, Spain.

³Department of Chemical Engineering, Aragon Institute of Nanoscience (INA), University of Zaragoza, Campus Río Ebro - Edificio I+D, C/ Poeta Mariano Esquillor S/N, 50018-Zaragoza, Spain.

⁴Sevilla Institute of Materials Science, Department of Inorganic Chemistry, University of Sevilla-CSIC, Américo Vespucio 49, 41092, Sevilla, Spain.

Corresponding author

*Prof. Teresita.F. Garetto
Predio CCT - Conicet Santa Fe
Colectora Ruta Nac. 168
3000 Santa Fe
Tel. 54 342 4511546
e-mail: tgaretto@fiq.unl.edu.ar
tgaretto@gmail.com*

Abstract

The performance of rotating metallic monolith stirrer reactor was studied for selective lactose oxidation in liquid phase at 65 °C, atmospheric pressure and with air as oxidant agent. The Au/Al₂O₃ deposition on metallic substrates was performed by wash-coating, producing catalyst coating thicknesses between 5 and 20 μm. Monoliths with different configuration (channel size between 0.36 and 1.06 mm) were used as stirrer blades in a batch reactor. Internal and external mass transfer limitations were observed during liquid phase lactose oxidation. For stirring rates equal or higher than 600 rpm there were no important external diffusional restrictions and this was also independent of the monolith configuration. Coating with thickness higher than 15 μm presents loss of catalyst effectiveness due to internal diffusional restrictions. Excellent stability in the catalytic tests was obtained after three regeneration-reaction cycles. Regeneration was carried out at 400 °C in air flow. Gold particle size distribution in the monolith washcoat, determined by TEM before and after reaction, was homogeneous with a medium size of around 5 nm. This is in agreement with the very good reproducibility and stability obtained in the catalytic tests. After calcination at 500°C, some sintering and a heterogeneous distribution of metal particle size was observed, accompanied by a slight loss in catalyst activity. It is concluded that metallic monolith stirrer reactors are a promising application for selective lactose oxidation in liquid phase.

Keywords:

Selective oxidation, lactose, gold nano-structured catalyst, metallic monolith, lactobionic acid

1. Introduction

The recovery of waste from the agri-food industry is a highly strategic way of meeting the challenge of the circular economy [1]. However, despite the studies carried out, the number of products on the market derived from this waste remains limited.

A case of high interest is whey; the liquid effluent from the cheese production. Non-processed whey causes an environmental problem due to its high biochemical (BOD) and chemical oxygen demand (COD) [2]. Lactose (LA) is an important by-product of the cheese and casein manufacture, whose production and global market had been estimated to about 1.4 million tons per year [3]. The relatively low water solubility and sweetness of LA, limits its use in many applications. Another restricting factor is the inability of LA intolerant people (who have a low level of lactase enzyme in the body) to digest milk sugar limiting its use in many applications [4]. However, as a consequence of its worldwide surplus and low cost, there is a great interest in the research of innovative processes for transforming LA, expanding its applications in the food and pharmaceutical industries as value-added derivatives. Some significant developments include the production of highly valued pharmaceutical products and functional food ingredients such as lactulose, lactitol, lactobionic acid, lactosucrose, and galacto-oligosaccharides [1-4].

Obtaining higher value-added products through catalytic processes, using LA from the cheese whey as raw material, is a challenging task. By selective oxidation of LA, lactobionic acid (LBA) can be obtained (Scheme 1). This acid has antioxidant, humectant and emollient properties, so it is widely used in formulations of the pharmaceutical, cosmetic and medicinal industry [4]. In addition, it is used in solutions for the preservation of human organs intended for transplant procedures [2].

In previous works, the oxidation of LA using Au catalysts supported on Al_2O_3 has been studied, and high conversions and high selectivity towards the production of LBA

were obtained. Generally, these studies have been done by heterogeneous catalysis in liquid phase, using powder catalysts and semi-batch reactors operating under continuous stirring [5-7]. The stirrer is used to provide mechanical energy required to mix or blend the reactants in such a way that the desired reaction or transfer process occurs at the desired rate. When using a stirred tank reactor for heterogeneous catalysis, the catalyst is usually added to the reaction system in the form of fine particles or powder. However, the use of powdered catalysts in this type of reactors can produce loss of activity by active phase leaching, diffusion limitations and operational problems such as filtering and re-use [7-9].

The problems related to using a slurry catalyst can be reduced significantly if the catalyst is immobilized in structured substrates [10-12]. Fixing the catalyst to a structured substrate (either by wash-coating or impregnation) is a possible solution. Moreover, the use of a structured catalyst as stirred blades combines the advantages of a structured substrate and catalytic stirrer. As structured substrates, monoliths have a promising application for liquid phase reaction due to their high geometric surface area and high void fraction, which provides accessibility of reactants to the catalyst particles with low pressure drop [11]. Another important benefit is that the safety is improved, because in case of reaction runaway fast shutting down is possible by stopping the impeller. The cordierite is the most common material for monolithic catalyst used as stirrer reactor [13-15]. Nevertheless, metallic monoliths are very interesting catalytic devices due to the possibility of obtaining thinner walls allowing higher cell density and, thus, higher geometric surface area [16]. The decreasing catalyst layer thickness with increasing cell density proved to be beneficial for the performance of the monolithic stirrer reactor [14]. This is very important, because thin catalyst layers may prevent internal diffusion

limitations. Therefore, the tuning ability of the catalytic layer thickness allows designing the monolithic catalyst for optimal activity and selectivity [8,14].

Although there are several works where the viability of structured systems is studied in multiphase reactions (hydrogenation of 3-methyl-1-pentyn-3-ol [8], synthesis of propylene carbonate [16], selective oxidation of cyclohexene [17], hydrogenation of edible oil [18]), there are no papers in the open literature, which analyze the behavior of monolithic structured catalysts used as a stirrer for LA oxidation. The aim of this work is to evaluate the performance of rotating metallic monoliths in a batch reactor for the selective LA oxidation to LBA. Wash-coating process was studied to coat monoliths with nano-structured Au/Al₂O₃ catalyst. The effect of stirring speed, monolith channel size and catalyst coating thickness on monolithic catalyst activity is studied. In addition, the optimization of thermal regeneration and the catalyst re-usability are analyzed.

2. Experimental

2.1. Preparation of powder catalyst.

Supported gold catalyst was prepared by the direct anionic exchange (DAE) method assisted by ammonia, as previously proposed by Ivanova et al. [19]. Firstly, the necessary quantity of HAuCl₄ (Johnson Matthey, >99.5%) to obtain 2wt% of supported gold was dissolved in 2 L of distilled water and then heated to 70°C. Once the final temperature was achieved, the support, a commercial γ -Al₂O₃ (Spheralite SCS 505, Procatalyse), was added to the solution and aged under vigorous stirring for another 20 min. Then, the suspension was cooled down and a concentrated ammonia solution, prepared with NH₃ (Aldrich), was added. After 20 min, the solid was filtered, washed with distilled water, dried at 100 °C and finally calcined at 300 °C for 4 h.

CAUTION NOTE: The use of ammonia can produce the gold ammonia complexes known as fulminating gold (olive green upon drying). The variation of the above mentioned procedure could be potentially dangerous.

2.2. Preparation of metallic substrates and structured catalysts.

Fecralloy® monoliths (25-mm diameter and 25-mm length) were prepared with different channel size. The geometric parameters of different monoliths are summarized in Table 1. Prior to coating, metallic monoliths were thermally treated in air during 22 h at 900 °C. Monoliths were coated by wash-coating with an aqueous slurry of powder Au/Al₂O₃ catalyst (20 wt%), with AL20-NYACOL® colloidal alumina (8.3 wt%) and polyvinyl alcohol (2.1 wt%) as additives. The slurry pH was adjusted at 4 to obtain a stable suspension [20]. The coating was repeated several times with a drying step (120 °C for 30 min) between coatings to deposit 250, 500 and 1000 mg of the catalyst on the metallic monoliths. Afterward, the wash-coated monoliths were calcined between 400 and 500 °C for 2 h in air. Finally, the average thickness of the catalyst layer was estimated as $\delta = w_{\text{cat}} \cdot \rho_{\text{cat}}^{-1} \cdot S_{\text{g}}^{-1}$, where w_{cat} is the amount of deposited catalyst, ρ_{cat} is the catalyst coating density (0.825 g·cm⁻³), and S_{g} is the geometric surface area of the monolith, resulting an average δ ranging from 5–30 μm (Table 1).

Coated samples are referred to as RX_Y_Z, where RX is the type of monolith (see Table 1); Y is the nominal catalyst load in mg (250, 500 or 1000); and Z is the catalyst coating thickness (μm).

2.3. Characterization techniques.

The zeta potential curve was determined with a ZETASIZER model NANO-Z from MALVERN INSTRUMENTS LTD. The powder catalyst (≈ 20 mg) was ultrasonically dispersed in an aqueous solution of 0.001 M NaCl and the pH was varied between 2 and 12 with nitric acid or ammonium hydroxide. A laser diffraction particle sizing technique (MALVERN MASTERSIZER 2000) was used to measure the powder catalyst particle distribution. 100 mg of the powder catalyst were dispersed in 20 mL distilled H₂O and the pH adjusted to 4, and promptly submitted to ultrasounds for 2 h to avoid undesired agglomerations. The viscosity of the catalyst slurry was measured in a rotational rheometer (TA INSTRUMENTS AR 1500 EX). The adherence of the catalyst layer deposited onto metallic monoliths was evaluated introducing the monoliths in vials with petroleum ether, sonicating for 30 min [21]. Excess of petroleum ether was removed by drying (100 °C for 1 h) and then calcining in air (450 °C for 2 h). Adherence of catalyst coating is expressed as the percentage of the catalytic loading that remains after ultrasonic test.

The textural properties of samples (powder and structured catalyst) were determined by N₂ physisorption at 77 K with a Micromeritics ASAP 2020. Prior to analysis, samples were degassed at 180 °C under a vacuum of 1.33 Pa for 2 h. Metal loading of samples was determined by inductively coupled plasma (ICP) using a Perkin Elmer OPTIMA 2100 equipment.

Electron microscopy observations were carried out at the LMA-INA-UNIZAR facilities using a Tecnai G2-F30 Field Emission Gun microscope with high angle annular dark field scanning transmission electron microscopy detector (HAADF-STEM) allowing a 0.2 nm point-to-point resolution and 0.1 line resolution operated at 300 kV. HAADF-STEM enables to acquire images with atomic number contrast for high scattering angles of the electrons (Z-contrast). Sample powder was dispersed in water by

ultrasonic bath, and a drop of this suspension was put over a copper grid coated with carbon film, and allowed to dry in air.

2.4. Catalytic tests.

Lactose (LA) oxidation in aqueous phase was carried out at 65 °C and atmospheric pressure in a thermostated glass reactor of 750 mL, equipped with a mechanical stirring system. The monoliths were attached by screws to the stirring system, what allows an easy disassembled. The objective is that the monoliths works as stirrer paddles in order to improve the contact between the reactive medium and the catalyst active phase. For regeneration, after a reaction cycle, monoliths were taken apart by unscrewing the mechanical attachment and then placed in a muffle furnace at the corresponding temperature, depending on the case. The initial LA (Anedra, 99%) concentration (C^0) was 0.014 M for all experiments and the catalyst mass to LA initial amount ratio (w/n^0) was 30 or 95 $\text{g}\cdot\text{mol}^{-1}$. Once the reaction temperature was reached, purified air (21% v/v O_2) was bubbled through the reaction mixture at a constant flow rate. The pH was adjusted at 9.0, which was already reported in previous works as the optimum pH for this reaction [5,6], using a 0.5 N NaOH (Cicarelli, 98%) aqueous solution. During the reaction, the pH value was kept constant using an automatic control system. Oxidation experiments were done varying the stirring rate between 200 and 700 rpm. Samples of reaction mixture were taken at regular intervals and analyzed using a Shimadzu HPLC equipment with refraction index detector. The chromatographic separation of LA and LBA was performed in a Phenomenex (Phenosphere 5 micras NH_2 , 80A 250mm, x 4.60 mm). A solution of acetonitrile and sodium phosphate buffer (50 mM, pH=5), both HPLC grade, were used as eluents. Only LA and LBA were detected and quantified in all of the experiments.

3. Results and discussion.

3.1. Monolithic catalyst preparation.

Wash-coating process by catalyst slurry is an excellent method to prepare structured catalyst [10]. First, the zeta potential was measured as a function of pH to identify the pH region for optimum dispersion of the Au/Al₂O₃ powder catalyst (Figure 1). The isoelectric point of the suspension occurred at pH 8.2. Zeta potential values higher than 30 mV were observed under acidic conditions (pH < 5), which is indicative of good particle dispersion [22]. Therefore, pH = 4 was selected for the catalyst slurry preparation. Another important parameter to increase of the slurry stability is the average particle size. In the literature, it was recommended that the average particle size should be below 10 μm [22]. In this regard, a dry-milling during 30 min was carried out to obtain the adequate particle size of Al₂O₃.

Several preliminary tests of the slurry formulation for wash-coating the metallic structured substrates were carried out following an experimental procedure. The coating characteristics (specific load, homogeneity and adhesion) were analyzed to choose the best recipe. In this sense, the selection of binder and stabilizer is crucial for the wash-coating of the structured substrates. It is well known that long-chain surfactants containing hydrophilic and hydrophobic groups, such as PVA, adsorb on the catalyst surface leading to steric stabilization of the slurry [23]. They are also able to reduce surface tension during drying process avoiding coating cracks and detachments [24]. Furthermore, binders like inorganic oxide colloid (Al₂O₃, CeO₂, ZnO, SiO₂) are used as thickeners to stabilize the slurry and also to promote the adherence between the catalyst and the substrate surface [25]. The additives and the solid content affect the viscosity of the catalyst slurry and this is probably the main parameter controlling the washcoating [ref 17]. Low viscosity values ensure easy coating and homogeneity but give rise to extremely low loads, and then numerous repeated coatings are required to reach the

desired catalyst load. But if viscosity is too high, problems of entry into the channels of the structured substrates and for removing additive excess uniformly without plugging the channels can occur. Thus, the recommended viscosity values for good coverage are between 10 and 20 cp [26]. Based on the foregoing, the following composition of slurry was selected: 12wt% of Au/Al₂O₃, 8.3wt% of colloidal alumina dispersion (binder) and 2.1 wt% of PVA (stabilizer), which at pH 4 gave a viscosity of 13.1mPa.s at 3400 s⁻¹. In Figure 2 it is shown that, over all of the structured substrates used in this work, the catalyst load increases almost linearly with the number of coatings. Also, it can be observed that the catalyst load depends on the monolith cell density: the higher the geometric surface area, the lower the number of coatings needed for a specific catalyst load. However, the specific catalyst loading per coating for all monoliths was $\approx 0.11 \text{ mg}\cdot\text{cm}^{-2}$. The wash-coating method used gives additive and homogeneous results, allowing for prepared three different nominal catalytic total loadings deposited on the metallic substrates: 250, 500 and 1000 mg.

On the other hand, the percentages of the catalyst loading that remains after the ultrasonic test were higher than 95%. Hence, the adhesion of the catalyst was excellent in all structured substrates and the coatings were homogeneous without plugging of monolith's channels (Figure 3), what is fundamental for this type of application in liquid phase.

The specific surface area of the slurry catalyst and the monolith coatings are presented in Table 2 and compared to that of the parent powder. It can be seen that the specific surface area of the slurry catalyst is lower than that of the parent catalyst. This is probably due to the incorporation of colloidal alumina with lower specific surface area ($\approx 190 \text{ m}^2\cdot\text{g}^{-1}$) in the slurry formulation. However, the catalyst coating textural properties were similar to the slurry catalyst.

3.2. Activity tests.

3.2.1. Influence of calcination temperature

Initially, monoliths with the major channel opening (R4_500_7) were chosen to test the activity and stability of the Au/Al₂O₃ nanostructured coating deposited on the metallic structure. For Au/Al₂O₃ powder catalysts used in lactose oxidation, Meyer et al. proposed as the best regeneration method the thermal treatment in air flow, because it allows cleaning the surface of the active sites covered by adsorbed species from reaction media [9]. Thus, several pairs of R4_500_7 monoliths were treated in air at temperatures between 400 and 500 °C for 2 hours and tested in the aqueous lactose oxidation at 65 °C, 450 rpm and $w/n^0 = 95 \text{ g}\cdot\text{mol}^{-1}$. These monoliths showed good activity, reaching a 100% lactose conversion in less than 120 min. Figure 4 shows initial reaction rate (r^0) of three consecutive cycles of reaction-regeneration (FA, I-R and II-R) as a function of the treatment temperature. It was determined that, for each treatment temperature, a slightly increased in the catalytic activity was observed after successive reaction-regeneration cycles, especially from sample FA to sample IR. This could be due to possible textural or structural modification of the active phase during these thermal treatments. A loss of activity was observed when the calcination-regeneration temperature was incremented from 400 °C to 500 °C. Indeed, the initial catalytic activity (r^0) was 0.145, 0.152 and 0.153 mmol·g⁻¹·min⁻¹, for the FA-IR-IIR sequence, when the thermal treatment of monoliths was at 400°C. When the monoliths treatment was carried out at 500 °C, the estimated r^0 values were 0.106, 0.118 and 0.120 mmol·g⁻¹·min⁻¹, i.e., lower than for samples treated and regenerated at 400 °C, what means an average decay of 20% for the initial activity. This behaviour was also verified analyzing the time necessary to reach a 50% conversion of lactose (not shown here). In summary, the best calcination-regeneration procedure of monoliths would be the treatment in air at 400°C during 2 h.

In order to explain these behaviour after three successive cycles of reaction-regeneration, samples of the nanostructured coating of R4_500_7 monoliths treated at 400 °C and 500°C were analysed by TEM. Micrographs and particle size distribution histograms of the samples when the regeneration was carried out at 400 °C, are presented in Figure 5 (A-D). Independently of the used magnification, and after counting more than 350 particles, it was verified that the main fraction of Au nanoparticles are between 3 and 10 nm in size, with a mode at 5 nm; only a very small fraction having sizes higher than 10 nm was detected (Figure 5 C and D).

Micrographs and histograms of the coating samples of R4_500_7 treated at 500 °C are presented in Figure 6 (A-D). In this case, a heterogeneous size distribution of the metallic Au nanoparticles could be observed (Figure 6 A and B). Precisely, the histograms, obtained by counting more than 300 particles from different regions in the sample, showed two clearly distinct distributions (Figure 6 C and D): a) regions with a bimodal distribution of Au nanoparticles between 7 and 32 nm, with modes around 10 nm and 15-20 nm (Figure 6C); b) regions with nanoparticles between 3 and 10 nm, with a mode around 3-5 nm (Figure 6D). These results are indicative that the treatment at 500 °C is leading to a selective sintering of the metallic Au phase, occurring and taking place in some regions of the support. It is likely that the interaction of metallic nanoparticles with the support depends on the type of Al₂O₃ surface on which Au is dispersed. As a consequence, a fraction of the metallic Au nanoparticles, the one that interacts more weakly with support surface, sinters more easily when regeneration treatment was carried out at 500°C instead of 400 °C. The cause for this selective sintering of the metallic Au nanoparticles could be the surface heterogeneity of Al₂O₃, probably generated during the wash-coating process. This heterogeneity gives place to two different type of regions: a) ones in which Au nanoparticles are strongly anchored on the support sites of greater

stability and remains as nano-crystallites of 3-6 nm in size; b) others in which Au nanoparticles are in low interaction with the support, and thus these metal particles can migrate and sinter to form Au particles with sizes greater than 10 nm. A similar behaviour was observed in a previous work when the interaction of Au with Al₂O₃ prepared by different methods was compared [27]. It is concluded that the activation of LA molecules over the surface of Au nanoparticles having around 5 nm or less is more effective than over the surface of Au nanoparticles with sizes higher than 10 nm. As a consequence, the activity of the exposed metallic Au surface after treatment of the monolith catalyst at 500 °C was some lower than the one obtained after treatment at 400 °C.

3.2.2. Reproducibility and stability tests.

Activity tests with different monolith pairs of the same channel configuration and thermal treated at 400 °C in air for 2 h were carried out. Figure 7 shows the evolutions of LA conversion as a function of time for three different pairs of R4_500_7 monoliths and three reaction-regeneration cycles. For a particular pair of monoliths, the same evolution of conversion vs time after each of the regenerations (I-R, II-R and III-R) was observed. This is, independently of the monolith pair chosen, the same r^0 ($\approx 0.15 \text{ mmol}\cdot\text{g}^{-1}\cdot\text{min}^{-1}$) and time for converting 50% or 100 % of LA were reached in each cycle. Even when the same comparison is made with the three different pairs of monoliths, the behavior described above is repeated. Briefly, the three pairs of monoliths showed the same catalytic activity even after three cycles of reaction-regeneration. Based on these results, we concluded that there is a very good reproducibility in the preparation of the Au/Al₂O₃ monolithic catalysts. That is to say that the coated monoliths preparation thereof is highly reproducible. In addition, it could be observed that after three regenerations at 400 °C, the metallic phase and its activity do not change, which indicates that the coated monoliths are stable when they are regenerated at this temperature. The reproducibility of the

catalytic performance after three cycles and the fact that no Au was detected by ICP in the liquid phase after each run are indicative that no leaching is occurring during liquid-phase lactose oxidation.

3.2.3. Influence of stirring rate on initial reaction rate

Experiments with different monolith configurations (R1_500_6, R2_500_7, R3_500_11 and R4_500_15) treated at 400°C in air for 2 h were done. Reaction temperature was fixed in 65°C and the ratio mass of catalyst to initial lactose moles (w/n^0) was 95 g·mol⁻¹. For all experiments the total catalyst mass employed was 1000 mg. Figure 8 shows the r^0 values as a function of the stirring rate. For all the monoliths configurations the maximum reaction rate achieved are similar (≈ 0.15 mmol·g⁻¹·min⁻¹) and it was accomplished for stirring rates in the range of 600 and 700 rpm. At this point, it is important to notice that, under the same conditions, the initial reaction rate estimated using the slurry catalyst with a stirring rate of 600 rpm was around 0.13 mmol·g⁻¹·min⁻¹, which is close to that obtained with monoliths (0.15 mmol·g⁻¹·min⁻¹) at the same stirring rate. These results indicate that for stirring rates equal or higher than 600 rpm, the catalytic activity is independent of the monolith channel configuration. Hence, it can be established that, at the experimental conditions used in this work, the kinetic of liquid-phase lactose oxidation is not affected by external diffusional restrictions when the stirring rate is around 600 rpm or higher. Instead, according to Figure 8, it is clear that for stirring rates lower than 500 rpm there is a strong influence of the monolith channel opening on the LA oxidation rate. The activity pattern observed below 500 rpm: R1 < R2 < R3 < R4, can be explained by considering that the gas-liquid flow is more restricted when the size of the channel is smaller, i.e., at low stirring rate this restriction becomes more influencing on the external mass transfer and thus on the global reaction rate. As the rpm increases, the restriction of the flow through the channels becomes less important,

and then the oxidation rate increases until it reaches the maximum. This also explains the fact that the maximum moves towards higher stirring rate as the channel becomes smaller.

The external mass transfer coefficients are increased with channel size and stirrer speed [28]. The overall effect of the increasing stirring speed is that the activity increases, because the flow through the monolithic channels increases with stirrer speed [14]. Hoek et al. observed that above 600 rpm the activity of 62 cpcc monolith ($d = 1.09$ mm) did not improve [14]. However, decreasing the channel diameter to 0.370 mm with metallic monolith, 700 rpm is necessary, in agreement with the trend observed in this work.

3.2.4. Effect of the catalyst layer thickness.

Taking into account that at 600 rpm there is no influence of the size of the channel (Figure 8) on the initial reaction rate, it was decided to check the existence of diffusive phenomena through the catalytic layer deposited on the monoliths (internal diffusion). Experiments were carried out for w/n^0 values of $30 \text{ g}\cdot\text{mol}^{-1}$ and $95 \text{ g}\cdot\text{mol}^{-1}$ and stirring rate of 600 rpm varying the thickness of the catalytic layer in the range from 6 to 28 μm (Figure 9-A). It was determined that for thicknesses less than 15 μm (monoliths R1_500_6, R2_500_7, R3_500_11 and R4_500_15), the reaction rates are similar, indicating that the diffusion through the catalytic layer would not be the controlling step. However, it was observed that when the thickness is greater than 15 μm (monolith R4_1000_28), the reaction rate decreases appreciably, which indicates the presence of internal diffusive phenomena in the catalyst layer controlling the lactose oxidation rate. It can be concluded that for layer thicknesses of up to 15 μm and working at stirring rates greater than or equal to 600 rpm, the control is chemical.

Figure 9-B shows the initial reaction rate for stirring rates of 450 and 600 rpm as a function of catalyst layer thickness for R4_250_8, R4_500_15 and R4_1000_28 monoliths. It is worth noting that the initial reaction rates are similar for both stirring

rates when thickness is less than or equal to 15 μm . Instead, for thicknesses greater than 15 μm (28 μm), the reaction rate values at 600 rpm is markedly higher than at 450 rpm. These results confirm the presence of diffusional limitations when the layer thickness is higher than 15 μm .

The thickness of the coating layers decreases with increasing cell density. Hoek et al. [14] observed that the activity per reactor volume clearly increases with increasing cell density. The higher specific surface area produce thinner catalyst coating and thus the internal mass transfer of reactive is enhanced. For foam stirrer reactor, an activity drop was observed with coatings thicker than 5 μm [8,29]. With this type of reactors, it is possible to enhance the gas-liquid mass transfer. However, the more restricted thickness limits and the low specific surface area of foam reactors respect to monolithics ones (1205 $\text{m}^2\cdot\text{m}^{-3}$ against 3433 $\text{m}^2\cdot\text{m}^{-3}$ for R4 configuration, see Table 1) do not allows the optimisation on the catalyst amount. Therefore, it can be said that catalyst coating thickness is a critical point in liquid phase reaction.

The results obtained in this work show that there is a limit to the amount of catalyst that can be coated to the monoliths. The amount of catalyst can be tuned by changing the number, length and diameter, and cell density of the monoliths. However, Hoek et al. [14] observed that there is a length limitation. The activity per reactor volume increases with the length of the monolithic structures due to the increase of the total amount of catalyst. Nevertheless, if the activity is normalised by surface area, the activity decreases with increasing length of the monolithic structures, becoming constant at a length of 0.03 m. The explanation of this result is that liquid entrance effect is beneficial for the external mass transfer, being more important in shorter monoliths [14,16]. Therefore, the best way to improve the structured catalyst activity in rotating stirrer reactor is to use metallic

monolith with high geometric surface area to obtain thin catalyst coating without diffusion limitations.

Conclusions

The nano-structure Au/Al₂O₃ monolithic catalysts obtained in this work, incorporated to the stirrer in a batch reactor, were active, stable and selective in the oxidation of lactose to lactobionic acid in aqueous phase. Thermal treatment in air at 400 °C, carried out during regeneration-reaction cycles, conduct to a stable metallic phase in which particle size is between 3 and 10 nm. Regeneration at 500 °C produces a selective sintering of Au metallic particles what slightly decrease the catalyst activity. The monolith cell density and the thickness of the catalyst layer influence the lactose oxidation rate in liquid phase due to external and/or internal mass diffusional restrictions. The reaction conditions and catalyst characteristics that allow working in chemical control were determined: stirring rates higher than or equal to 600 rpm and catalyst thickness less than or equal to 15 µm. The catalyst thickness that can be obtained in monoliths is higher than those than can be reached on foams, what allows an optimization of the final catalyst load.

Acknowledgments.

We thank the Universidad Nacional del Litoral (UNL), Consejo Nacional de Investigaciones Científicas y Técnicas (CONICET) and Agencia Nacional de Promoción Científica y Tecnológica (ANPCyT) from Argentina, the Basque Government (IT1069-16) and the Spanish MINECO/FEDER (ENE2015-66975-C3-3-R and CTQ2015-73901-JIN) for the financial support of this work.

References

- [1] A.S. Matharu, E.M. de Melo, J.A. Houghton, Opportunity for high value-added chemicals from food supply chain wastes, *Biores Technol* 215 (2016) 123-129.
- [2] R.E. Shepherd, Y. Issacson, L. Chensny, S. Zhang, R. Kortés, K. John, Lactobionic and gluconic acid complexes of Fe^{II} and Fe^{III}; control of oxidation pathways by an organ transplantation preservant, *J. Inorg. Biochem.* 49 (1993) 23-48.
- [3] L-F. Gutierrez, S. Hamoudi, K. Belkacemi, Lactobionic acid: A high value-added lactose derivative for food and pharmaceutical applications, *Int. Dairy J.* 26 (2012) 130-111.
- [4] E. Berardesca, F. Distanto, G.P. Vignoli, C. Oresajo, B. Green, Alpha hydroxyacids modulate stratum corneum barrier function, *British J Dermat* 137(1997) 934-938.
- [5] C.I. Meyer, S.A. Regenhart, J. Zelin, V. Sebastian, A.J. Marchi, T.F. Garetto, A kinetic modeling of the liquid-phase oxidation of lactose over Pt- and Au- supported catalysts, *Top. Catal.* 59 (2015) 168-177.
- [6] E.V. Murzina, A. V. Tokarev, K. Kordás, H. Karhu, J.-P. Mikkolaa, D. Yu. Murzin, D-Lactose oxidation over gold catalysts, *Cat. Today* 131 (2008) 385-392.
- [7] N. Meyer, D. Pirson, M. Devillers, S. Hermans, Particle size effects in selective oxidation of lactose with Pd/h-BN catalysts, *Appl. Catal. A: General* 467 (2013) 463-473.
- [8] M.A. Leon, T.A. Nijhuis, J. van der Schaaf, J.C. Schouten, Mass transfer modeling of a consecutive reaction in rotating foam stirrer reactors: Selective hydrogenation of a functionalized alkyne, *Chem. Eng. Sci.* 73 (2012) 412-420.
- [9] N. Meyer, C. Renders, R. Lanckman, M. Devillers, S. Hermans, Gold as active phase of BN-supported catalysts for lactose oxidation, *Appl. Catal. A: General* 504 (2015) 549-558.
- [10] F. Visscher, J. van der Schaaf, T.A. Nijhuis, J.C. Schouten, Rotating reactors - A review, *Chem. Eng. Res. Des.* 91 (2013) 1923-1940.
- [11] R.K.E. Albers, M.J.J. Houterman, T. Vergunst, E. Grolman. J.A. Moulijn, Novel monolithic stirrer reactor, *A.I.Ch.E. Journal* 44 (1998) 2459–2464.
- [12] K. Pangarkar, T.J. Schildhauer, J.R. van Ommen, J. Nijenhuis, F. Kapteijn, J.A. Moulijn, Structured Packings for Multiphase Catalytic Reactors, *Ind. Eng. Chem. Res.* 47 (2008) 3720-3751.
- [13] K.M. De Lathouder, J.J.W. Bakker, M.T. Kreutzer, S.A. Wallin, F. Kapteijn, J.A. Moulijn, Structured reactors for enzyme immobilization: A monolithic stirrer reactor for application in organic media, *Chem. Eng. Res. and Des.* 84 (2006) 390-398.
- [14] I. Hoek, T.A. Nijhuis, A.I. Stankiewicz, J.A. Moulijn, Performance of the monolithic stirrer reactor: applicability in multi-phase processes, *Chem. Eng. Sci.* 59 (2004) 4975-4981.
- [15] J. Zhu, F. Wu, M. Li, J. Zhu, J. G. van Ommen, L. Lefferts, Influence of internal diffusion on selective hydrogenation of 4-carboxybenzaldehyde over palladium catalysts supported on carbon nanofiber coated monolith, *Appl. Catal. A: General* 498 (2015) 222-229.
- [16] D. Wu, Y. Guo, S. Geng, Y. Xia, Synthesis of propylene carbonate from urea and 1,2-propylene glycol in a monolithic stirrer reactor, *Ind. Eng. Chem. Res.* 52 (2013) 1216–1223.
- [17] O. Sanz, F.J. Echave, F. Romero-Sarria, J.A. Odriozola, M. Montes, Advances in structured and microstructured catalytic reactors for hydrogen production, in: L.M. Gandia, G. Arzamedi, P.M. Dieguez (Eds.), *Renewable Hydrogen Technologies: Production, Purification, Storage, Applications and Safety*, Elsevier 2013, pp. 201-224.

- [18] M.T. Alotaibi, M.J. Taylor, D. Liu, S.K. Beaumont, G. Kyriakou, Selective oxidation of cyclohexene through gold functionalized silica monolith microreactors, *Surf. Sci.* 646 (2016) 179-185.
- [19] S. Ivanova, C. Petit, V. Pitchon, A new preparation method for the formation of gold nanoparticles on an oxide support, *Appl. Catal. A: General* 267 (2004) 191-201.
- [20] T. Boger, M.M.P. Zieverink, M.T. Kreutzer, F. Kapteijn, J.A. Moulijn, W.P. Addiego, Monolithic catalysts as an alternative to slurry systems: Hydrogenation of edible oil, *Ind. Eng. Chem. Res.* 43 (2004) 2337-2344.
- [21] S. Yasaki, Y. Yoshino, K. Ihara, K. Ohkubo, Method of manufacturing an exhaust gas purifying catalyst, US Patent 5208206, 1993.
- [22] C. Agrafiotis, A. Tsetsekou, The effect of powder characteristics on washcoat quality. Part I: alumina washcoats, *J. Eur. Ceram. Soc.* 20 (2000) 815-824.
- [23] T.C. Patton, *Paint Flow and Pigment Dispersion: a Rheological Approach to Coating and Ink Technology*, 2nd ed.; Wiley: New York; Chichester, 1979.
- [24] L. C. Almeida, F. J. Echave, O. Sanz, M. A. Centeno, J. A. Odriozola, M. Montes, Washcoating of Metallic Monoliths and Microchannel Reactors. *Stud. Surf. Sci. Catal.* 175 (2010) 25-33.
- [25] F.J. Echave, O. Sanz, M. Montes, Washcoating of microchannel reactors with PdZnO catalyst for methanol steam reforming, *Appl. Catal. A: General* 474 (2014) 159-167.
- [26] X. D. Xu, J. A. Moulijn, Preparation of Monolithic Catalysts by Dip Coating, in *Prep. Catal. VII* 1998, 118, pp. 845-854
- [27] A-F. An, A-H. Lu, Q. Sun, J. Wang, W-C. Li, Gold nanoparticles stabilized by a flake-like Al₂O₃ support, *Gold Bull.* 44 (2011) 217-222.
- [28] H.P. Kritzinger, B.C. Decider, C.R. Kleijn, J.J. Derksen, H.E.A. van den Akker, Turbulent flow in a stirred tank with permeable impeller blades, *Proceeding of FEDSM 2002 Montreal, Quebec, Canada.*
- [29] M.A. Leon, R. Tschentscher, T.A. Nihjuis, J. van der Schaaf, J.C. Schouten, Rotating foam stirrer reactor: Effect of catalyst coating characteristics on reactor performance, *Ind. Eng. Chem.* 50 (2011) 3184-3193.

Table 1. Geometric parameters of the different Fecralloy® metallic structured substrates (monoliths) employed.

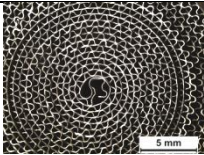
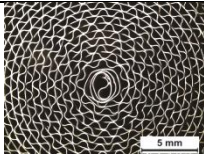
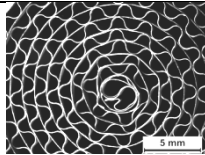
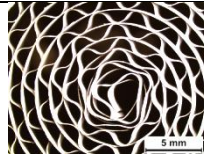
Monolith type				
	R1	R2	R3	R4
Geometric surface (cm ²)	940	825	540	424
Specific surface area (m ² ·m ⁻³)	8640	6965	4312	3433
Hydraulic diameter (μm)	361	475	827	1065
Porosity (%)	78	83	89	91
cpc (cells·cm ⁻²)	363	214	72	45

Table 2. Textural properties of powder and coating catalysts.

Sample	Catalyst coating thickness (μm)	S_{BET} ($\text{m}^2 \cdot \text{g}^{-1}$)	V_{pore} ($\text{cm}^3 \cdot \text{g}^{-1}$)	D_{pore} (nm)
Parent catalyst	-	242	0.44	7.3
Slurry catalyst	-	229	0.43	7.5
R4_250_7	7	227	0.42	7.5
R4_1000_28	28	229	0.43	7.5

Captions to Figures

Scheme 1: Oxidation of lactose (LA) to lactobionic acid (LBA)

Figure 1. Evolution of electrical Z-potential as a function of the Au/Al₂O₃ slurry pH.

Figure 2. Amount of catalyst loaded over the different metallic structured substrates (R1 to R4) as a function of the number of coatings.

Figure 3. Optic image of different metallic structured substrate configurations (monoliths) coated with ~500 mg of catalyst per monolith.

Figure 4. Initial oxidation reaction rate of lactose (r^0) in liquid phase as a function of calcination-regeneration temperature: ■ calcinated monolith (FA), ■ first regeneration (I-R), ■ second regeneration (II-R). Reaction conditions: 65 °C, 450 rpm, $w/n_0 = 95 \text{ g} \cdot \text{mol}^{-1}$, pH= 9.0.

Figure 5. TEM micrographs of nanostructured Au/Al₂O₃ deposited on metallic monoliths (A and B), and metallic particle size distribution histograms (C and D) after three cycles of reaction at 65 °C and regeneration at 400 °C.

Figure 6. TEM micrographs of nanostructured Au/Al₂O₃ deposited on metallic monoliths (A and B) and metallic particle size distribution histograms (C and D) after three cycles of reaction at 65 °C and regeneration at 500 °C.

Figure 7. Lactose conversion as a function of time corresponding to three different pairs of monoliths subjected to cycles of reaction (65 °C, 600 rpm, 0.011 M, 750 mL) and regeneration (400 °C in air for 2 h). □ after first regeneration (I-R), ○ after second regeneration (II-R), Δ after third regeneration (III-R).

Figure 8. Influence of stirring rate on initial lactose reaction rate corresponding to monolith configurations: □ R1_500_6, ○ R2_500_7, Δ R3_500_11 and ▽ R4_500_15. Reaction conditions: 65 °C, $w/n_0 = 95 \text{ g}\cdot\text{mol}^{-1}$, pH = 9.0.

Figure 9. Effect of catalyst layer thickness on initial lactose reaction rate. (A) Reaction conditions: 65 °C, $w/n_0 = 30$ and $95 \text{ g}\cdot\text{mol}^{-1}$, 600 rpm. (B) Reaction conditions: 65 °C, $w/n_0 = 30 \text{ g}\cdot\text{mol}^{-1}$, ■ 450 and ■ 600 rpm.

Scheme 1

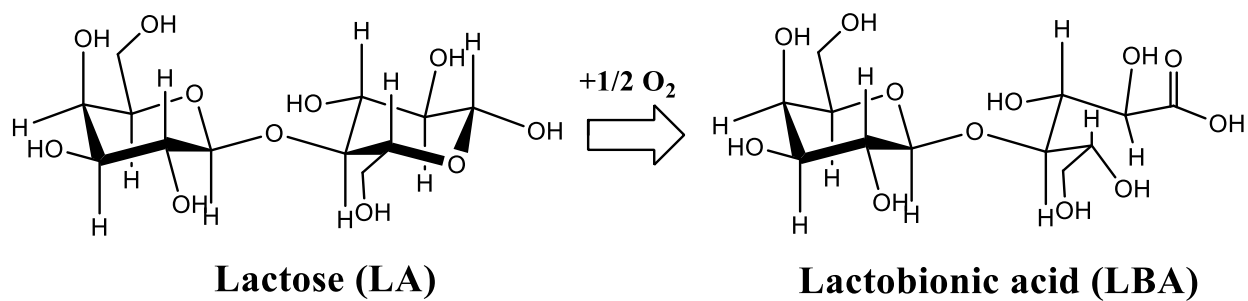


Figure 1

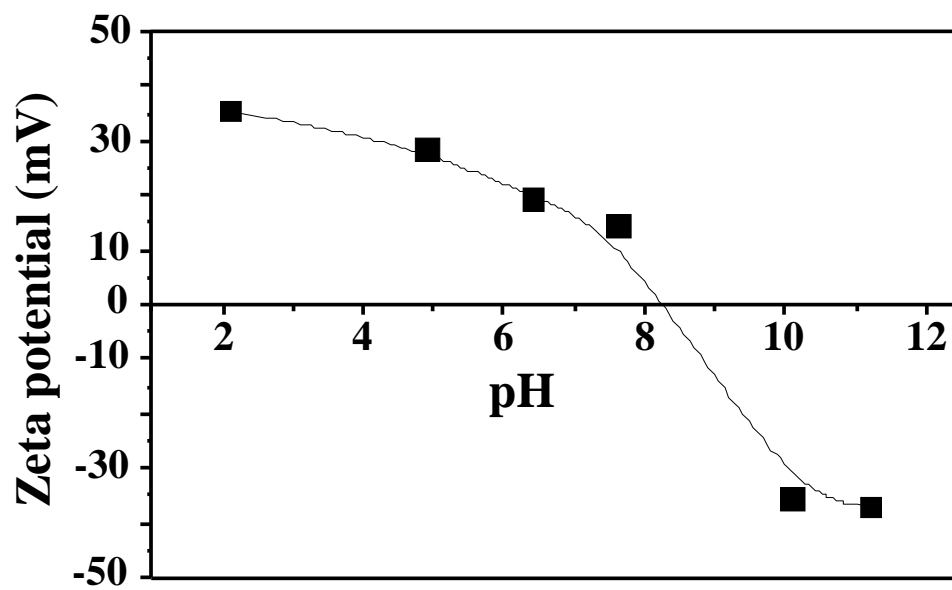


Figure 2

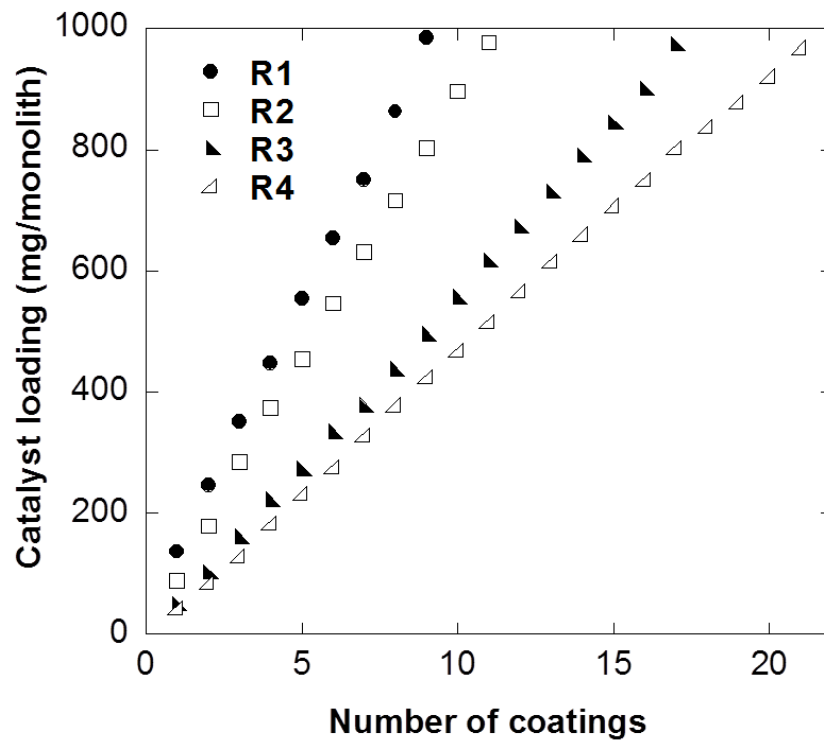


Figure 3

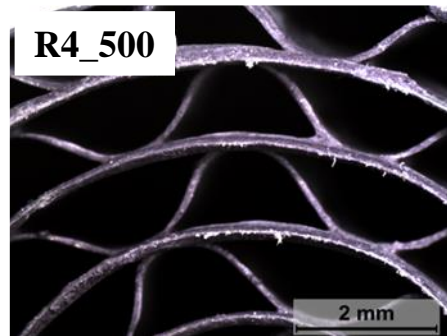
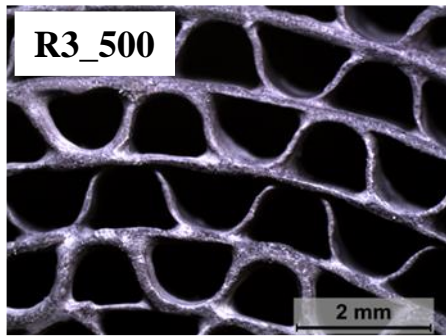
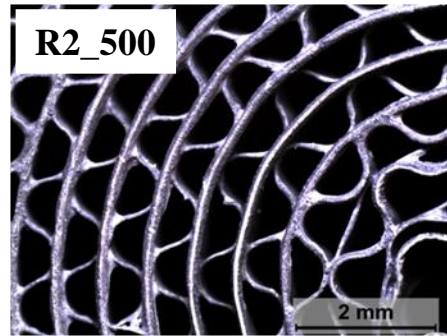
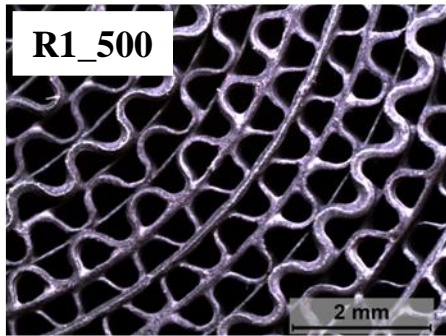


Figure 4

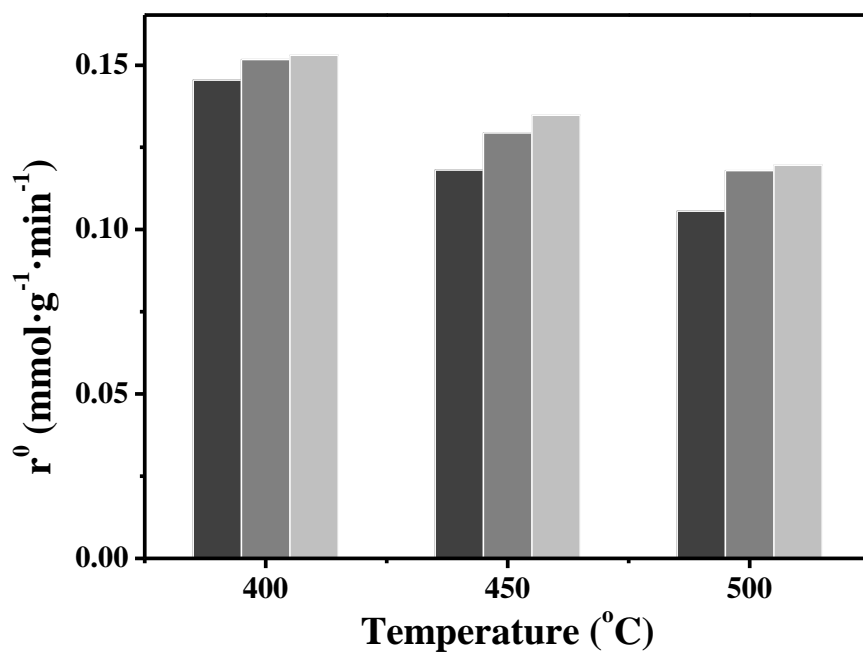


Figure 5

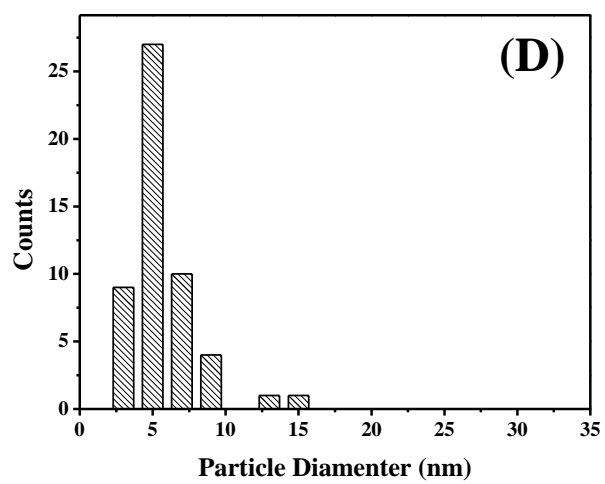
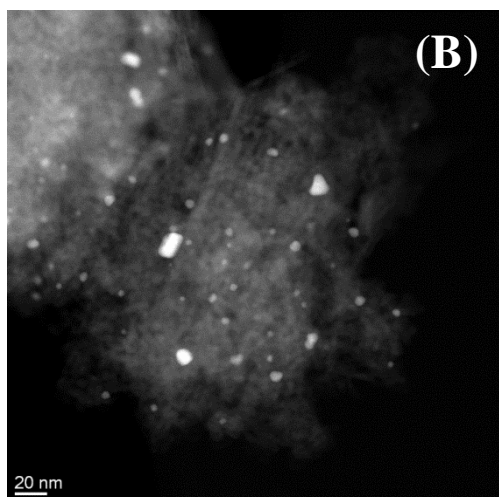
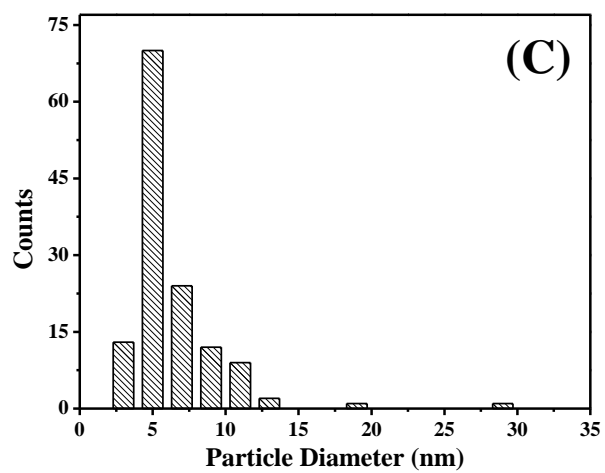
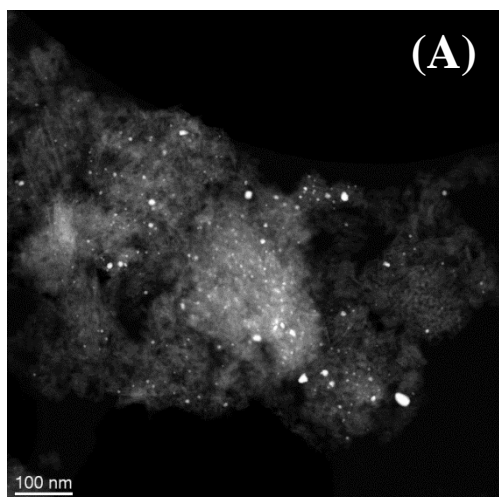


Figure 6

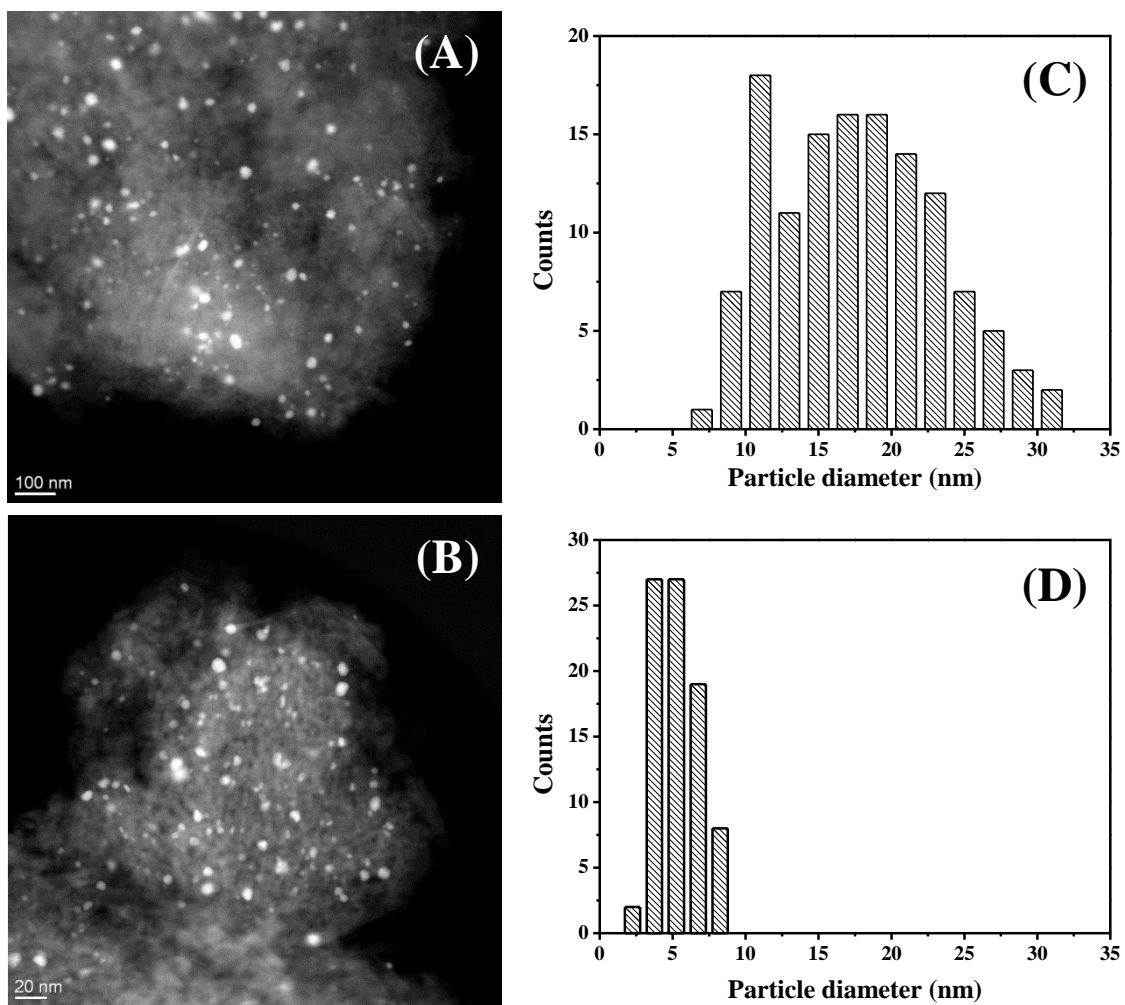


Figure 7

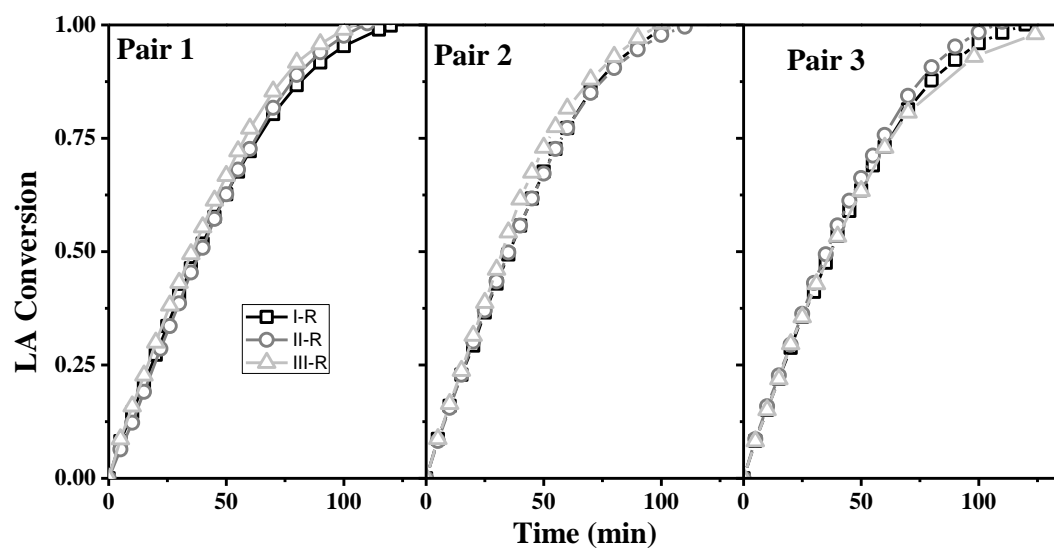


Figure 8

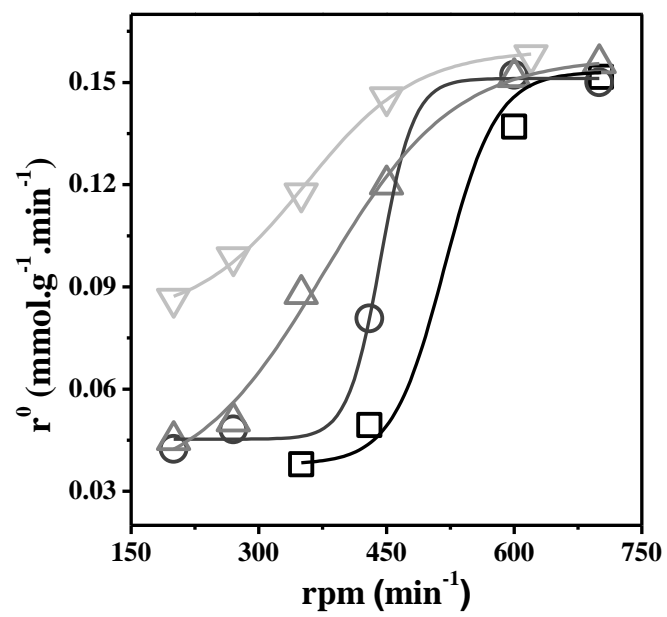


Figure 9

